The Cu-CHA deNOx Catalyst in Action: Temperature-Dependent NH3-Assisted Selective Catalytic Reduction Monitored by Operando XAS and XES

(Article begins on next page)

17 April 2024

The Cu-CHA deNO$_X$ catalyst in action: temperature-dependent NH₃-SCR monitored by *operando* X-ray Absorption and Emission Spectroscopies

Kirill A. Lomachenko[†,‡], Elisa Borfecchia[*,†], Chiara Negri[†], Gloria Berlier[†], Carlo Lamberti[†,‡], Pablo Beato[§], Hanne Falsig[§], Silvia Bordiga[†]

[†]Department of Chemistry, NIS Centre and INSTM Reference Center, University of Turin, via P. Giuria 7, 10125 Turin, Italy.

[‡]IRC "Smart Materials", Southern Federal University, Zorge Street 5, 344090 Rostov-on-Don, Russia.

[§]Haldor Topsøe A/S, Haldor Topsøes Allé 1, 2800 Kgs. Lyngby, Denmark.

Supporting Information Placeholder

ABSTRACT: The small-pore Cu-CHA zeolite is today the object of intensive research efforts aiming to rationalize its outstanding performance in the NH₃-assisted selective catalytic reduction (SCR) of harmful nitrogen oxides and to unveil the SCR mechanism. Herein we exploit *operando* X-ray spectroscopies to monitor the Cu-CHA catalyst *in action* during NH₃-SCR in the 150-400 °C range, targeting Cu oxidation state, mobility and preferential N or O ligation as a function of reaction temperature. By combining *operando* XANES, EXAFS and vtc-XES, we unambiguously identify two distinct regimes for the atomic-scale behavior of Cu active-sites. Low-temperature SCR, up to ca. 200 °C, is characterized by balanced populations of Cu(I)/Cu(II) sites and dominated by mobile NH₃-solvated Cu-species. From 250 °C upwards, in correspondence to the steep increase in catalytic activity, the largely dominant Cu-species are framework-coordinated Cu(II) sites, most likely representing the active sites for high-temperature SCR.

Recent years have seen a Renaissance for metal-exchanged zeolites. These systems are attracting growing interest as versatile platforms for novel chemistry at the boundary between homogeneous and heterogeneous catalysis. Copper, with its rich redox chemistry and exquisite coordinative flexibility, as we see in many Cu-enzymes,[1,2] is the ideal candidate for single-site catalysis empowered by host-guest interactions inside the zeolite cages. In particular, the small-pore Cu-CHA zeolite is today the object of intensive research efforts aiming to rationalize its outstanding performance in the NH₃-assisted selective catalytic reduction (SCR) of harmful nitrogen oxides.[3-7] Cu-CHA is currently commercialized due to its enhanced activity, selectivity and hydrothermal stability[8] with respect to other zeolite-based catalysts. Nonetheless, despite the recent advances in the understanding of the SCR mechanism on Cu-CHA,[6,9-15] several questions still need to be addressed to design deNO$_x$ catalysts able to keep pace with the increasingly stricter regulations worldwide.

The powerful experimental and theoretical methods matured in the last decade are enabling an unprecedented molecular-level understanding of the structure-composition-activity relationship in Cu-zeolites. Very recently, Schneider and co-workers[15] have synergized experiment and theory to correlate the macroscopic compositional parameters in Cu-CHA and the types and numbers of Cu-sites formed after dehydration and in SCR-relevant conditions. The authors provided direct evidences that during dehydration Cu(II) ions first populate *2Al* sites in the 6-membered rings (*6r*) of the CHA framework (Z₂−Cu(II), where Z₂ denotes 2 neighboring charge-balancing framework Al sites), identified as the most energetically favoured exchange sites for "naked" Cu(II) ions.[16,17] Once the less reducible[11,15,18,19] Z₂−Cu(II) sites are saturated, Cu cations are stabilized in proximity of isolated *1Al* sites as redox-active

Z−[Cu(II)OH⁻] complexes (where Z denotes an isolated framework Al site), representing the largely dominant coordination environment at high Cu-loading.[19,20] Very importantly to the present study, the chemical and spectroscopic distinction between these two types of Cu-sites is much less pronounced when the catalyst is exposed to the SCR feed or partial mixtures of SCR reactants. Consistently with previous reports,[21,22] *operando* XANES during SCR at 200 °C revealed the presence of a ca. 50/50% Cu(I)/Cu(II) mixture. Paolucci *et al.*[15] associated the Cu(I) and Cu(II) components to the most stable species evidenced by DFT: Z[Cu(I)(NH₃)₂] (also observed after exposure to the NO+NH₃ mixture at 200 °C, as was reported before[12,13,23]) and Z[Cu(II)OH(NH₃)₃] on *1Al* sites; Z₂[Cu(II)(NH₃)₄] and ZNH₄⁺/Z[Cu(I)(NH₃)₂] on *2Al* sites. On this basis, NH₃-solvated Cu-complexes, scarcely interacting with CHA framework and poorly influenced by Al distribution, are proposed as the SCR active sites at 200 °C. On the other hand, the authors suggest that NH₃ de-solvation at higher temperature is expected to influence the SCR rates, especially in the oxidation half-cycle. Since no evidences on this key aspect have been reported so far, a temperature-dependent investigation of the Cu-CHA catalyst *in action* during NH₃-SCR becomes crucial to pinpoint alternative reaction pathways and Cu active species as a function of the operation temperature. To bridge this gap, we monitored Cu-CHA during NH₃-SCR in the 150−400 °C range by *operando* XAS and XES. As illustrated in a number of recent reviews,[5,7,24] these X-ray spectroscopies[25-31] are ideal to track the properties of Cu cations in zeolites, and allowed us to determine (i) oxidation state, (ii) mobility and (iii) preferential N or O ligation for Cu-active sites as a function of reaction temperature. From these experiments it clearly emerges that temperature strongly influences Cu-speciation during SCR, with profound implications on the elucidation of SCR active sites and mechanism. We performed *operando* XAS/XES during standard SCR (500 ppm NO, 500 ppm NH₃, 5% H₂O, 10% O₂/He, flow rate = 300 ml/min) using a well-established gas flow setup on a Cu-CHA catalyst with composition (Si/Al=15, Cu/Al=0.48) equivalent to the one investigated in our previous studies[13,19,23] and selected by Paolucci *et al.*[15] as the reference for *1Al* type-containing Cu-CHA. Additional details on sample synthesis and experimental setup are reported in SI, Section 1). A mass spectrometer downstream the reactor cell allowed us to verify that the catalyst was effectively active for SCR reaction during XAS/XES measurements, with temperature-dependent NO conversion in qualitative agreement with SCR rates obtained in dedicated laboratory catalytic tests on the same catalyst batch (see also SI, Section 2).
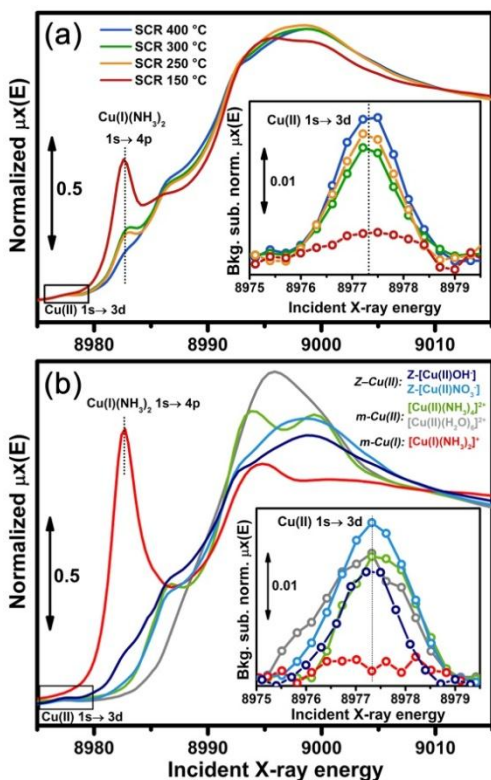
2

Figure 1. (a) *Operando* XANES collected during standard SCR at temperatures of 150, 250, 300, 400 °C. (b) XANES spectra of selected reference Cu-species employed to interpret *operando* data reported in part (a). The same vertical and horizontal axes scale is used in part (a) and (b) to facilitate a direct comparison between *operando* and reference data. The insets report a magnification of the background-subtracted Cu(II) 1s → 3d pre-edge peaks highlighted by the black boxes in the main panels.

Figure 1 shows the temperature-dependent modifications in the XANES of Cu-CHA during SCR. To guide data interpretation, *operando* XANES (Figure 1a) are compared to the ones obtained for a series or references (Figure 1b), selected considering the principal spectral features emerging during SCR. Reference XANES spectra were separately measured for Cu(I) and Cu(II) aqua/amino complexes in solution (*m-Cu(I)* and *m-Cu(II)*, *m* = "mobile") and framework-interacting Cu(II) species in Cu-CHA (*Z-Cu(II))*, namely three-coordinated Z−[Cu(II)OH⁻] and four-coordinated Z−[Cu(II)(NO₃)⁻] (see SI, Section 3.1). To estimate temperature-dependent Cu-speciation during SCR, we applied linear combination fit (LCF) analysis using the reference spectra in Figure 1b (see SI , Section 3.2). The *operando* SCR XANES spectrum at 150 °C is in excellent agreement with the observations reported by Paolucci *et al.* and others[15,21,22] during standard SCR at 200 °C. Hence, our experimental conditions guarantee a reliable comparison with previous studies. The pre-edge peak at ca. 8977.3 eV, mostly arising from Cu(II) 1s → 3d transition,[32,33] is significantly lower than in Cu(II) references. The characteristic edge-rising peak at ca. 8982.5 eV deriving from 1s → 4p transition in the linear Cu(I)(NH₃)₂ complex[32,34,35] is well evident. LCF indicates a ca. 46% contribution from *m-Cu(I),* in the form of [Cu(I)(NH₃)₂]⁺, whereas the remaining XANES signal is fitted with an almost equal fraction of *Z-Cu(II)* (ca. 26%) and *m-Cu(II)* (ca. 25%) species. In other words, 'mobile' Cu(II) and Cu(I) sites solvated by ammonia are the main sites, in agreement with Paolucci *et al.*,[15] with a small fraction of Cu(II) sites interacting with the framework. Crucially, an abrupt modification in the *operando* XANES is observed from 250 °C and upwards. The contribution of *m-Cu(I)* reduces to ca. 15% and the spectral shape evolves towards the one characteristic of *Z-Cu(II)*: an edge-rising shoulder at ca. 8986.6 eV and a broad

white line peak centered at 8997.7 eV, typically increasing in intensity for four-coordinated *Z-Cu(II)* sites with respect to three-coordinated ones (*e.g.* comparing the Z-[Cu(II)OH⁻] and Z-[Cu(II)NO₃⁻] references in Figure 1b).[13,19] *Z-Cu(II)* species collectively account for ca. 74% of Cu sites (the remaining 11% attributed to minor contributions from *m-Cu(II)* complexes). The remarkable intensity increase of the Cu(II) 1s → 3d pre-edge peak clearly indicates a largely dominant 2+ oxidation state, in agreement with LCF results. A further increase in the operation temperature induces more subtle but still appreciable modifications. At 350 °C, the relative contributions from mobile and framework-interacting species remain substantially unchanged, whereas the slight intensity decrease observed in the white line region is compatible with the partial conversion of four-coordinated *Z-Cu(II)* sites into three-coordinated ones. This trend is maintained at 400 °C. Here LCF evidences negligible contributions from *m-Cu(I)* and *m-Cu(II)* species, and largely dominant *Z-Cu(II)* sites preferentially occurring as three-coordinated sites.
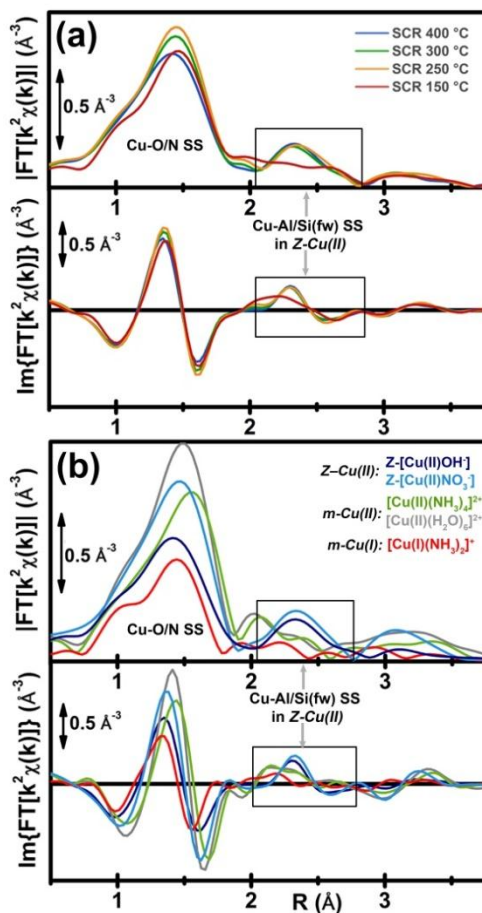

Figure 2. (a) *Operando* phase-uncorrected FT-EXAFS spectra (moduli and imaginary parts of FT in top and bottom panel, respectively) collected during standard SCR at temperatures of 150, 250, 300, 400 °C. (b) Phase-uncorrected FT-EXAFS spectra of selected Cu-references employed to interpret *operando* data reported in part (a). In both part (a) and (b) all the FT-EXAFS spectra are calculated transforming k²-weighted χ(k) spectra in the range 2.5-12.4 Å⁻¹ (see SI, Section 4) and plotted using the same vertical and horizontal axes scale to facilitate a direct comparison between *operando* and reference data.

Operando EXAFS and XES allowed us to independently validate the XANES results described above, targeting the mobility level and the preferential O or N ligation of the Cu active sites, respectively. It is now established[13,15,19,21] that the well-defined maximum peaking at ca. 2.3 Å in the phase-uncorrected modulus

3

of FT-EXAFS spectrum of dehydrated Cu-CHA derives from single-scattering paths involving Al/Si atoms of the CHA framework. Although the variable-temperature data collection and the presence of multiple Cu-species prevent a quantitative fitting of *operando* EXAFS, the second-shell peak at 2.3 Å can be exploited as a fingerprint for framework-coordinated Cu-sites. As shown in Figure 2a, this EXAFS feature is always present during SCR in the (250−400) °C range, with stable intensity and shape comparable with what observed for *Z-Cu(II)* references reported in Figure 2b. In the same temperature interval, we notice slight fluctuations in the first-shell intensity of the *operando* EXAFS spectra, suggesting an increase in the average first-shell coordination number as temperature decreases. Interestingly, in the high-R range, the FT-EXAFS at 250 °C seems more similar to what seen in the Z-[Cu(II)NO₃⁻] reference, where the presence of a well-defined maximum at ca. 3.2 Å was connected multiple-scattering scattering feature peculiar of bidentate Z−[Cu(II)(NO₃)₃⁻] moieties[13] (see SI, Section 4). The EXAFS signature of the Cu-CHA catalyst drastically changes when SCR is run at 150 °C. The second-shell maximum is strongly perturbed and partially evolves towards the unstructured shape characteristic of *m-Cu(I)/(II)* species. The first shell intensity decreases despite the drop of thermal contribution to the Debye-Waller factors, consistently with an increase of the fraction of two-coordinated species with N/O ligands, which are hardly distinguishable by XAS. As already shown in *in situ/operando* studies on Cu-CHA,[14,23,36] such an ambiguity regarding the type of ligands can be resolved by valence-to-core (vtc) XES, monitoring the energy position of the weak Kβ" satellite.[28,37] Moreover, the overall Kβ₂,₅ line shape is highly sensitive to local coordination geometry and symmetry and represents a valid support to qualitatively cross-check Cu-speciation from XANES.

Figure 3 shows *operando* Cu-CHA XES spectra for key temperature points during SCR (Figure 3a), together with representative reference XES data for *Z-Cu(II)*, *m-Cu(II)* and *m-Cu(I)* species formed inside the pores of Cu-CHA (Figure 3b), see also SI Sections 1.4 and 3. As for *operando* XANES and EXAFS datasets, two distinct regimes can be individuated. In the high-temperature range, at 400 and 300 °C, the Kβ₂,₅ line shape characteristic of *Z-Cu(II)* species is observed, and the energy position of the Kβ" peak reveals largely dominant O-ligation. Conversely, at 150 °C the Kβ₂,₅ line shape clearly evolves towards the one observed for the Cu(I)(NH₃)₂ reference, characterized by a narrow and intense peak at ca. 8976 eV. In parallel, the Kβ" satellite significantly shifts to higher energy, unambiguously indicating a substantial increase in the fraction of N-coordinated Cu-species in the catalyst. The Kβ" energy position observed in these conditions is intermediate between the ones observed for pure O- and pure N-ligation, in agreement with XANEX LCF analysis (60% of NH₃-solvated Cu-species, largely present as [Cu(I)(NH₃)₂]²⁺, 46%). In addition, the broad feature on the low-energy side of the Kβ₂,₅ peak, typical of hydrated Cu(II) ions (see Figure 3b, gray curve), is never observed in the *operando* XES series, supporting a very minor H₂O coordination in the whole probed temperature range. Consistently with LCF XANES and with many FTIR evidences reported before,[23,38] in the low-temperature SCR range Cu-ions are almost exclusively solvated and mobilized by NH₃.
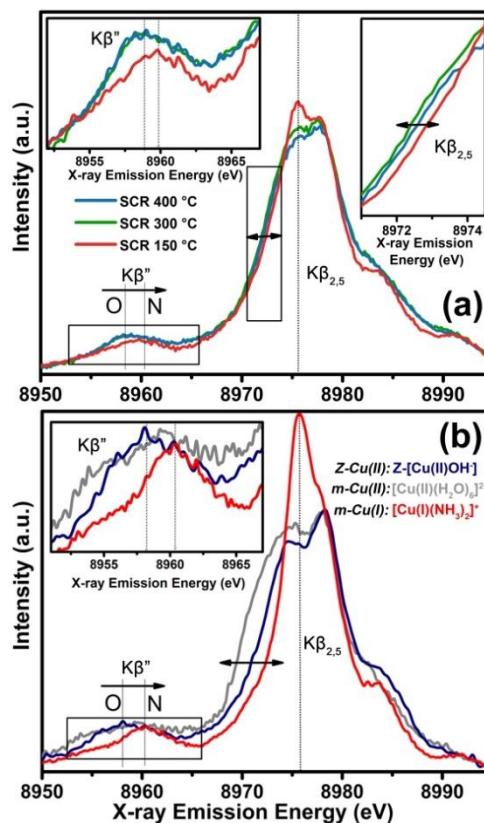

Figure 3. (a) Background-subtracted *operando* XES spectra collected during standard SCR at temperatures of 150, 300, 400 °C. (b) Background-subtracted XES spectra of selected Cu references states formed inside the pores of Cu-CHA, representative of *Z-Cu(II)*, *m-Cu(II)* and *m-Cu(I)* species. The insets report magnifications of the Kβ" satellites and, for part (a) only, of the left side of the Kβ₂,₅ line, highlighted by the black boxes in the main panels.

In conclusion, *operando* XAS/XES during SCR unambiguously point out that two distinct regimes exist for the atomic-scale behavior of Cu-sites in the investigated Cu-CHA catalyst, emerging at different temperature ranges. As depicted in Figure 4, low-temperature SCR, up to ca. 200 °C, is characterized by balanced populations of Cu(I)/Cu(II) sites and dominated by mobile NH₃-solvated Cu-species. We fully agree with Paolucci *et al.*[15] in assigning the Cu(I) component to Z[Cu(I)(NH₃)₂] species. As for the Cu(II) component, assigned by Paolucci *et al.* to Z[Cu(II)OH(NH₃)₃] species, results of our LCF analysis demonstrate that it can be as well ascribed to a complex mixture of residual O-bonded *Z-Cu(II)* sites and *m-Cu(II)* complexes (mostly with NH₃ ligands). In the 250−400 °C range, a completely different scenario is revealed: Cu is largely present as framework-coordinated *Z-Cu(II)* species, accounting for ca. 70% to more than 90% of total Cu sites. Here, temperature-dependent dynamics seems to mostly involve Cu interaction with O-bonding extra-framework groups and reactants from the gas-phase (*e.g.* hydroxyls and bidentate nitrates/nitrites), while coordination to framework is substantially unperturbed. Very interestingly, the transition between these two regimes corresponds to the steep rise in the temperature-dependent SCR conversion rate, determined in a dedicated catalytic test (see SI, Section 1.2) and reported in Figure 4 for comparison. These novel findings evidence a profound influence of the operation conditions on Cu-speciation during NH₃-SCR, which should be considered to fully unleash the potential of Cu-zeolite based deNOₓ catalysts.
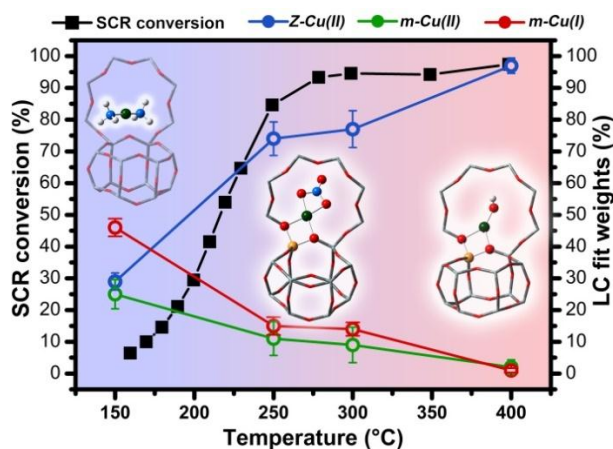
Figure 3. Comparison between temperature dependent NH₃-SCR conversion rate and Cu-speciation in Cu-CHA. Structural snapshots of the dominant Cu-species evidenced by LCF analysis of *operando* XANES for each probed temperature are also reported (atoms color code: Cu: green, O: red, Al: yellow, Si: gray, N: blue, H: white).

ASSOCIATED CONTENT

Supporting Information

The Supporting Information is available free of charge via the Internet at http://pubs.acs.org. Experimental details; MS during *operando* X-ray spectroscopy; LCF analysis of *operando* XANES; Additional details on *operando* EXAFS spectra.

AUTHOR INFORMATION

Corresponding Author

*elisa.borfecchia@unito.it

Notes

The authors declare no competing financial interests.

ACKNOWLEDGMENT

REFERENCES

(1)   Solomon, E. I.; Heppner, D. E.; Johnston, E. M.; Ginsbach, J. W.; Cirera, J.; Qayyum, M.; Kieber-Emmons, M. T.; Kjaergaard, C. H.; Hadt, R. G.; Tian, L. *Chem. Rev.* **2014**, *114*, 3659.

(2)   Lee, J. Y.; Karlin, K. D. *Curr. Opin. Chem. Biol.* **2015**, *25*, 184.

(3)   Brandenberger, S.; Krocher, O.; Tissler, A.; Althoff, R. *Catal. Rev.* **2008**, *50*, 492.

(4)   Granger, P.; Parvulescu, V. I. *Chem. Rev.* **2011**, *111*, 3155.

(5)   Deka, U.; Lezcano-Gonzalez, I.; Weckhuysen, B. M.; Beale, A. M. *ACS Catal.* **2013**, *3*, 413.

(6)   Gao, F.; Kwak, J.; Szanyi, J.; Peden, C. F. *Top. Catal.* **2013**, *56*, 1441.

(7)   Beale, A. M.; Gao, F.; Lezcano-Gonzalez, I.; Peden, C. H. F.; Szanyi, J. *Chem. Soc. Rev.* **2015**, *44*, 7371.

(8)   Kwak, J. H.; Tran, D.; Burton, S. D.; Szanyi, J.; Lee, J. H.; Peden, C. H. F. *J. Catal.* **2012**, *287*, 203.

(9)   Kwak, J. H.; Lee, J. H.; Burton, S. D.; Lipton, A. S.; Peden, C. H. F.; Szanyi, J. *Angew. Chem.-Int. Edit.* **2013**, *52*, 9985.

(10)   Gao, F.; Walter, E. D.; Kollar, M.; Wang, Y.; Szanyi, J.; Peden, C. H. F. *J. Catal.* **2014**, *319*, 1.

(11)   Gao, F.; Washton, N. M.; Wang, Y. L.; Kollar, M.; Szanyi, J.; Peden, C. H. F. *J. Catal.* **2015**, *331*, 25.

(12)   Paolucci, C.; Verma, A. A.; Bates, S. A.; Kispersky, V. F.; Miller, J. T.; Gounder, R.; Delgass, W. N.; Ribeiro, F. H.; Schneider, W. F. *Angew. Chem.-Int. Edit.* **2014**, *53*, 11828.

(13)   Janssens, T. V. W.; Falsig, H.; Lundegaard, L. F.; Vennestrøm, P. N. R.; Rasmussen, S. B.; Moses, P. G.; Giordanino, F.; Borfecchia, E.; Lomachenko, K. A.; Lamberti, C.; Bordiga, S.; Godiksen, A.; Mossin, S.; Beato, P. *ACS Catal.* **2015**, *5*, 2832.

(14)   Gunter, T.; Carvalho, H. W. P.; Doronkin, D. E.; Sheppard, T.; Glatzel, P.; Atkins, A. J.; Rudolph, J.; Jacob, C. R.; Casapu, M.; Grunwaldt, J. D. *Chem. Commun.* **2015**, *51*, 9227.

(15)   Paolucci, C.; Parekh, A. A.; Khurana, I.; Di Iorio, J. R.; Li, H.; Albarracin Caballero, J. D.; Shih, A. J.; Anggara, T.; Delgass, W. N.; Miller, J. T.; Ribeiro, F. H.; Gounder, R.; Schneider, W. F. *J. Am. Chem. Soc.* **2016**, *138*, 6028.

(16)   Korhonen, S. T.; Fickel, D. W.; Lobo, R. F.; Weckhuysen, B. M.; Beale, A. M. *Chem. Commun.* **2011**, *47*, 800.

(17)   Deka, U.; Juhin, A.; Eilertsen, E. A.; Emerich, H.; Green, M. A.; Korhonen, S. T.; Weckhuysen, B. M.; Beale, A. M. *J. Phys. Chem. C* **2012**, *116*, 4809.

(18)   Godiksen, A.; Stappen, F. N.; Vennestrom, P. N. R.; Giordanino, F.; Rasmussen, S. B.; Lundegaard, L. F.; Mossin, S. *J. Phys. Chem. C* **2014**, *118*, 23126.

(19)   Borfecchia, E.; Lomachenko, K. A.; Giordanino, F.; Falsig, H.; Beato, P.; Soldatov, A. V.; Bordiga, S.; Lamberti, C. *Chem. Sci.* **2015**, *6*, 548.

(20)   Giordanino, F.; Vennestrom, P. N. R.; Lundegaard, L. F.; Stappen, F. N.; Mossin, S. L.; Beato, P.; Bordiga, S.; Lamberti, C. *Dalton Trans.* **2013**, *42*, 12741.

(21)   McEwen, J. S.; Anggara, T.; Schneider, W. F.; Kispersky, V. F.; Miller, J. T.; Delgass, W. N.; Ribeiro, F. H. *Catal. Today* **2012**, *184*, 129.

(22)   Bates, S. A.; Verma, A. A.; Paolucci, C.; Parekh, A. A.; Anggara, T.; Yezerets, A.; Schneider, W. F.; Miller, J. T.; Delgass, W. N.; Ribeiro, F. H. *J. Catal.* **2014**, *312*, 87.

(23)   Giordanino, F.; Borfecchia, E.; Lomachenko, K. A.; Lazzarini, A.; Agostini, G.; Gallo, E.; Soldatov, A. V.; Beato, P.; Bordiga, S.; Lamberti, C. *J. Phys. Chem. Lett.* **2014**, *5*, 1552.

(24)   Lomachenko, K. A.; Borfecchia, E.; Bordiga, S.; Soldatov, A. V.; Beato, P.; Lamberti, C. *J. Phys.: Conf. Ser.* **2016**, *712*, 012041.

(25)   Bordiga, S.; Groppo, E.; Agostini, G.; van Bokhoven, J. A.; Lamberti, C. *Chem. Rev.* **2013**, *113*, 1736.

(26)   Mino, L.; Agostini, G.; Borfecchia, E.; Gianolio, D.; Piovano, A.; Gallo, E.; Lamberti, C. *J. Phys. D-Appl. Phys.* **2013**, *46*, 423001.

(27)   Garino, C.; Borfecchia, E.; Gobetto, R.; Salassa, L.; van Bokhoven, J. A.; Lamberti, C. *Coord. Chem. Rev.* **2014**, *277–278* 130.

(28)   Glatzel, P.; Bergmann, U. *Coord. Chem. Rev.* **2005**, *249*, 65.

(29)   Smolentsev, G.; Soldatov, A. V.; Messinger, J.; Merz, K.; Weyhermuller, T.; Bergmann, U.; Pushkar, Y.; Yano, J.; Yachandra, V. K.; Glatzel, P. *J. Am. Chem. Soc.* **2009**, *131*, 13161.

(30)   Singh, J.; Lamberti, C.; van Bokhoven, J. A. *Chem. Soc. Rev.* **2010**, *39*, 4754.

(31)   *X-Ray Absorption and X-ray Emission Spectroscopy: Theory and Application*; van Bokhoven, J. A.; Lamberti, C., Eds.; John Wiley & Sons: Chichester (UK), 2016.

(32)   Kau, L. S.; Spirasolomon, D. J.; Pennerhahn, J. E.; Hodgson, K. O.; Solomon, E. I. *J. Am. Chem. Soc.* **1987**, *109*, 6433.

(33)   Sano, M.; Komorita, S.; Yamatera, H. *Inorg. Chem.* **1992**, *31*, 459.

(34)   Lamble, G.; Moen, A.; Nicholson, D. G. *J. Chem. Soc. Farady Trans.* **1994**, *90*, 2211.

(35)   Mathisen, K.; Stockenhuber, M.; Nicholson, D. G. *Phys. Chem. Chem. Phys.* **2009**, *11*, 5476.

(36)   Günter, T.; Doronkin, D. E.; Boubnov, A.; Carvalho, H. W. P.; Casapu, M.; Grunwaldt, J.-D. *Top. Catal.* **2016**, 1.

(37)   Vegelius, J. R.; Kvashnina, K. O.; Klintenberg, M.; Soroka, I. L.; Butorin, S. M. *J. Anal. At. Spectrom.* **2012**, *27*, 1882.

(38)   Lezcano-Gonzalez, I.; Deka, U.; Arstad, B.; Van Yperen-De Deyne, A.; Hemelsoet, K.; Waroquier, M.; Van Speybroeck, V.; Weckhuysen, B. M.; Beale, A. M. *Phys. Chem. Chem. Phys.* **2014**, *16*, 1639.

Table of Contents artwork